Journal Pre-proofs



CRISPR-Cas12a powered multifunctional DNA nanodumbbell lock biosensor for multiple molecular detection

Yuqing Zhu, Xiaohe Zheng, Rui Zhu, Hongrui Zhao, Hongli Zhai, Feiyang Qian, Tenghua Zhang, Zihui Xie, Silan Liu, Bowen Jiang, Yan Sheng, Jiaming Hu

PII: S1385-8947(23)02225-8
DOI: https://doi.org/10.1016/j.cej.2023.143494
Reference: CEJ 143494

To appear in: *Chemical Engineering Journal*

Received Date: 6 March 2023
Revised Date: 20 April 2023
Accepted Date: 10 May 2023

Please cite this article as: Y. Zhu, X. Zheng, R. Zhu, H. Zhao, H. Zhai, F. Qian, T. Zhang, Z. Xie, S. Liu, B. Jiang, Y. Sheng, J. Hu, CRISPR-Cas12a powered multifunctional DNA nanodumbbell lock biosensor for multiple molecular detection, *Chemical Engineering Journal* (2023), doi: https://doi.org/10.1016/j.cej.2023.143494

This is a PDF file of an article that has undergone enhancements after acceptance, such as the addition of a cover page and metadata, and formatting for readability, but it is not yet the definitive version of record. This version will undergo additional copyediting, typesetting and review before it is published in its final form, but we are providing this version to give early visibility of the article. Please note that, during the production process, errors may be discovered which could affect the content, and all legal disclaimers that apply to the journal pertain.

© 2023 Elsevier B.V. All rights reserved.

CRISPR-Cas12a powered multifunctional DNA nanodumbbell lock biosensor for multiple molecular detection

Yuqing Zhu[a,†], Xiaohe Zheng[b,†], Rui Zhu[a], Hongrui Zhao[a], Hongli Zhai[a], Feiyang Qian[a], Tenghua Zhang[a], Zihui Xie[a], Silan Liu[a], Bowen Jiang[a] Yan Sheng[a,*] and Jiaming Hu[a,*]

[a] MOE Key Laboratory of Laser Life Science & Institute of Laser Life Science, Guangdong Provincial Key Laboratory of Laser Life Science, College of Biophotonics, South China Normal University, Guangzhou 510631, China.

[b] Department of Laboratory Medicine, The First Affiliated Hospital, Sun Yat-sen University, Guangzhou 510080, China.

* Corresponding authors at: MOE Key Laboratory of Laser Life Science & Institute of Laser Life Science, Guangdong Provincial Key Laboratory of Laser Life Science, College of Biophotonics, South China Normal University, Guangzhou 510631, China.

E-mail addresses: ysheng@m.scnu.edu.cn (Y. Sheng), jmhu@m.scnu.edu.cn (J. Hu)

† These authors contributed equally.

Journal Pre-proofs

Abstract

Detection of multiple biomarkers for accurate diagnosis of disease is highly desirable but remains challenging. Here, we developed a versatile diagnostic biosensor (SMARTLOCK) through the unique combination of DNA tetrahedron, nonlinear HCR and CRISPR-Cas12a system for simultaneous detection of multiple nucleic acids, small molecules, proteins and different types of combinations. Two DNA tetrahedrons are assembled into a functional dumbbell lock, which was unlocked by the target molecules, thereby triggering a two-stage signal amplification of nonlinear HCR and CRISPR-Cas12a to generate powerful fluorescence signals. The capability of multi-target simultaneous detection of SMARTLOCK is demonstrated in the detection of miR-141, miR-375, miR-21, ATP, cortisol, insulin and their combinations. SMARTLOCK could selectively (specificity = 93.3%) and sensitively (sensitivity = 90%) distinguish early-stage prostate cancer (PCa) patients (n = 10) from healthy donors (n = 30). Measurement of two PCa-related RNAs (miR-141 and miR-375) shows the potential of SMARTLOCK to be a highly accurate and low-cost tool for the screening, diagnosis and prognosis of various diseases.

Keywords: CRISPR-Cas12a, DNA Nanotechnology, Fluorescence, Biosensor

1. Introduction

Nucleic acids, small molecules and proteins have been widely used as biomarkers since their aberrant expressions are closely associated with the occurrence and progression of various diseases, such as cancer, diabetes and cardiovascular disease. The current methods for measuring nucleic acids, small molecules and proteins, such as quantitative reverse transcription polymerase chain reaction (qRT-PCR) [1] , next-generation sequencing (NGS) [2] , microarrays [3] and enzyme-linked immunosorbent assay (ELISA) [4] generally require complex sample preparation, lengthy sample-to-result times and sophisticated measurement devices. Notably, single biomarker is not sufficient for accurate diagnosis, especially in early-stage disease [5, 6] . Therefore, it is desirable to develop a diagnostic biosensor capable of detecting several biomarkers of the same kind (for example: nucleic acids, small molecules or proteins), or even a combination of several different types of biomarkers in an accurate, highly effective and inexpensive manner.

DNA tetrahedron is a kind of 3D nanostructure that can be rapidly assembled by annealing four designed single-stranded DNAs, and each vertex can be readily functionalized with different

Journal Pre-proofs

chemical moieties and biomolecules [7, 8] . In the past years, DNA tetrahedron has demonstrated superior advantages in sensor construction [9] , drug delivery [10] , and molecular logic gates [11, 12] . In sensor construction, tetrahedron has been attached to the surface of magnetic beads or electrodes to enhance molecular recognition efficiency [13, 14] . Furthermore, the vertex DNA fragment complementary to the substrate could trigger hybridization chain reaction (HCR) for signal amplification [15, 16] . HCR can be divided into two categories: linear HCR and nonlinear HCR. Nonlinear HCR, as a highly dimensional HCR, tends to self-assembly to dendritic or branched DNA nanostructures with exponential growth kinetics under the trigger of the initiator sequence. Given the advantages of its enzyme-free, high-order growth kinetic, high sensitivity, and simple operation, nonlinear HCR is regarded as a powerful signal amplifier for the detection of biomarkers [17] . Linear HCR reactions are only at the one-dimensional level and may not provide sufficient sensitivity when it comes to identifying and tracking targets [18] . Compared with one-dimensional linear HCR, nonlinear HCR has greatly improved the detection performance, especially the detection sensitivity and selectivity.

CRISPR-Cas (clustered regularly interspaced short palindromic repeats and CRISPR-associated protein) systems have been widely harnessed for gene editing [19] , transcription regulation [20] and molecular diagnostics [21] . CRISPR-Cas12a is a class of RNA-guided nucleases that are activated by single-or double-stranded DNA targets, and one activated Cas12a could non-specifically cleave nearby thousands of single-stranded DNAs (named trans-or collateral cleavage effect) [22] . In recent years, some strategies have been developed in combination with CRISPR-Cas12a to realize signal amplification for sensitive detection of nucleic acids [23-25] , small molecules [26-29] or proteins [30] , however, few has been reported on multiplex detection. Moreover, most of these techniques require pre-amplification and various enzymes, which are cumbersome, expensive and time-consuming. To the best of our knowledge, there has been no report on integrating DNA tetrahedron, nonlinear HCR with CRISPR-Cas12a to simultaneously detect multiple nucleic acids, small molecules and/ or proteins for high signal gain.

Here, we describe SMARTLOCK (specific multifunctional DNA tetrahedron nanostructure unlocking), an in vitro multifunctional biosensor with femtomolar sensitivity based on DNA tetrahedron, nonlinear HCR and Cas12a-mediated collateral cleavage of a DNA reporter, allowing for detection of multiple nucleic acids, small molecules and/ or proteins simultaneously. MiR-141, miR-375 and miR-21 have been found to be effective biomarkers for prostate cancer [31-33] . Abnormal expression of adenosine triphosphate (ATP) and cortisol is closely associated with the development of many diseases, such as Parkinson's disease, depression, Addison's disease and cardiovascular disease [34, 35] . Insulin is a protein hormone secreted by insulin beta cells that lowers the blood glucose concentration through various metabolic pathways, and its disruption leads to the development of diabetes [36] . Thus, we select these nucleic acids, small molecules and proteins as model biomarkers to validate our assay. We demonstrate its performance for signal amplification and the potential to detect early-stage prostate cancer. Our findings indicate that SMARTLOCK provides a new perspective in the field of multiplex detection.

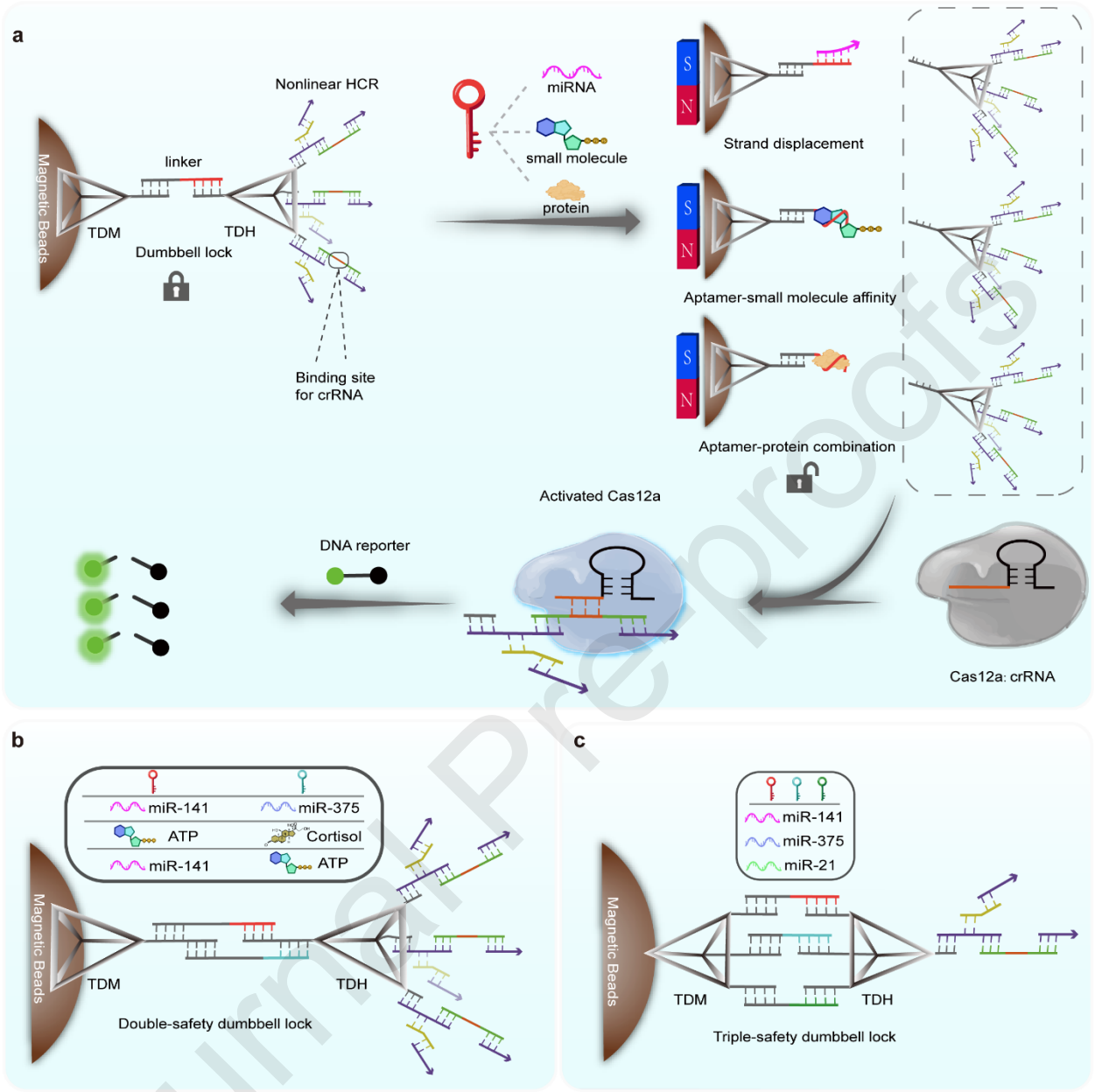


Figure 1. Working principle of SMARTLOCK. (a) Schematic illustration of the workflow of SMARTLOCK for detecting single target molecule. (b) Schematic illustration of double-safety dumbbell lock for detection of dual-target molecules. (c) Schematic illustration of triple-safety dumbbell lock for detection of trial-target molecules.

2. Materials and methods

2.1. Reagents

All oligonucleotides were synthesized and purified by Hippobio Co., Ltd. (Huzhou, China) and the sequences are listed in **Table S1**. N-(3-Dimethylaminopropyl) -N-ethylcarbodiimide hydrochloride (EDC), 2-(N-morpholino) ethanesulfonic acid, 4-morpholineethanesulfonic acid

Journal Pre-proofs

(MES), PBS buffer, hydrochloric acid (HCl) and Magnesium chloride ($MgCl_2$) were purchased from Sangon Biotech (Shanghai, China), insulin and ATP were purchased from Sigma-Aldrich (Louis, MO). Dopamine hydrochloride, cortisol was purchased from Aladdin Biochemical Technology Co., Ltd. (Shanghai, China), rCutSmart™ buffer was purchased from NEB (Beijing, China). All solutions used in the experiments were prepared using ultrapure water (resistance >18 MΩ cm), which was obtained through a Millipore Milli-Q ultrapure water system. Cas12a protein was donated by Prof. Jin Wang from the Institute of Translational Medicine, The First Affiliated Hospital of Shenzhen University.

2.2. Construction of dumbbell lock

DNA tetrahedron (TDM and TDH) consists of T1M, T2M, T3M, T4M (T1H, T2H, T3H, T4H) the equimolar ratio of four strands were mixed in TM buffer (20 mM Tris, 50 mM $MgCl_2$, pH 8.0) heated at 95 ℃ for 5 min and then quickly cooled to 4 ℃ within 1 min. In order to prepare nonlinear HCR, three components of DNA strands (strand A, strand B, strand C) (50 μM each) were dissolved in PBS buffer and incubated at 37 ℃ for 1.5 h. 2 μL 10 mg/ mL of magnetic beads were suspended in 400 μL MES buffer, and then the assembled TDM and 8 mg EDC were added. After incubation for 3 h with gentle shaking, the resulting magnetic beads-DNA tetrahedron complexes were separated by a magnetic stand with 1x TE buffer (10mM Tris-HCl, 1Mm EDTA, pH 8.0). The linkers, TDH and nonlinear HCR were then connected in 1x PBS buffer solution following the steps described above. It is worth noting that DNA tetrahedrons, nonlinear HCR are completed by pre-assembly and then ligated.

2.3. Fluorescence Analysis

Different concentrations of the target were added to the reaction system (1x rCutsmart™), incubated for 1 h, and then the supernatant was collected through the magnetic rack. The collected supernatant was then added to the Cas12a system (50 nM Cas12a, 100 nM crRNA) which has been incubated for 15 min, followed by the addition of DNA reporter (1 μM). The fluorescence measurements were carried out on Quant Studio 3 (Thermo Fisher Scientific).

2.4. Gel Electrophoresis

All gel electropherograms were made with a 2% agarose gel by weighing 0.5 g of agarose into 25 mL of 1xTAE (40 mM Tris-acetate, 2.0 mM EDTA, pH 8.5) and heating until the solution was clarified, then Gel Red as the oligonucleotide dye. Each lane contains 4 μL of sample-loading complex, run at 110 V for 40 min at room temperature. After electrophoresis, the gel was captured using the Gel Doc XR+ (Bio-Rad). The concentration of DNA in all gel electrophoresis experiments was 1 μM.

Journal Pre-proofs

2.5. Flow Cytometry Experiments

T1M-FAM has been modified with fluorescent group FAM, and appropriate amounts of T1M-FAM, T2M, T3M and T4M were added to 1 x TM buffer (20 mM Tris, 50 mM $MgCl_2$, pH 8.0) and heated to 95 ℃ for 5 min and then quickly lowered to 4 ℃ for use. 2 μL 10 mg/ mL beads were then connected to the magnetic beads using the method described above. Fluorescence was then collected by flow cytometer (Beckman Coulter, CytoFLEX).

2.6. Atomic Force Microscopy Characterization Experiment

40 μL of fresh 0.5% APTES solution was carefully deposited onto the center of the sheet and incubated for 2 min. The sheet was then washed thrice with ultrapure water to remove any residual APTES solution and dried using nitrogen gas. Next, 20 μL of pre-assembled TDM solution (80 nM) was added to the center of the mica surface.

2.7. Serum RNA Extraction

Total RNA was extracted from 200 μL of serum samples using the miRcute Total RNA Kit (DP503, Tiangen) according to the instruction of manufacturer. Samples were eluted in 30 μL nuclease-free water. Extracted samples were aliquoted and stored at -80 ℃.

2.8. Statistical analysis

All experiments and assays were repeated at least three times. The data were expressed as mean ± s.d. and compared by Student's t test. The GraphPad Prism version 5.0 and Origin 9 were used for data analysis. All of the illustrations were generated using Adobe Illustrator CC 2019.

3. Result and discussion

3.1. Design of SMARTLOCK

Figure 1a shows an overall illustration of SMARTLOCK and how it works. A specific dumbbell lock is designed, consisting of two DNA tetrahedrons, named TDM and TDH, respectively, conjugated by a linker complementary to the vertex DNA fragments of the two tetrahedrons. In addition, the other three vertex DNA fragments of TDM are modified with amino groups to connect with magnetic beads, while the other three vertex DNA fragments of TDH are designed to trigger nonlinear HCR reactions. In the absence of target molecule, the dumbbell lock is in its non-active configuration with a dumbbell-shaped structure, and the products of nonlinear HCR are firmly attached to the magnetic beads through the dumbbell lock, blocking the downstream reaction. In the presence of target molecule, the complementary or aptamer domain of linker can specifically bind with target molecule, consequently, the double-stranded DNA formed by linker and the vertex DNA fragment of TDH will unwind, unlocking the dumbbell lock,

Journal Pre-proofs

which releases TDH linked with the products of nonlinear HCR (TDH-nonlinear HCR complex). After magnetic separation, the supernatant containing the released TDH-nonlinear HCR complex was collected to participate in the downstream reaction with Cas12a: crRNA binary complex. The designed crRNA contains two regions: a repeat sequence and a guide sequence. The repeat sequence is an essential part for crRNA to anchor Cas12a enzyme and the guide sequence is complementary to the binding site of the products of nonlinear HCR. When the binding sites of nonlinear HCR products hybridize with Cas12a: crRNA binary complex, the collateral cleavage ability of Cas12a will be activated to cleave multiple DNA reporter probes, thereby generating amplified fluorescence signals. On this basis, we have further developed a double-safety dumbbell lock for simultaneous detection of dual-target molecules and a triple-safety dumbbell lock for trial-target molecules (**Figure 1b, c**).

3.2. Characterization and Optimization of SMARTLOCK

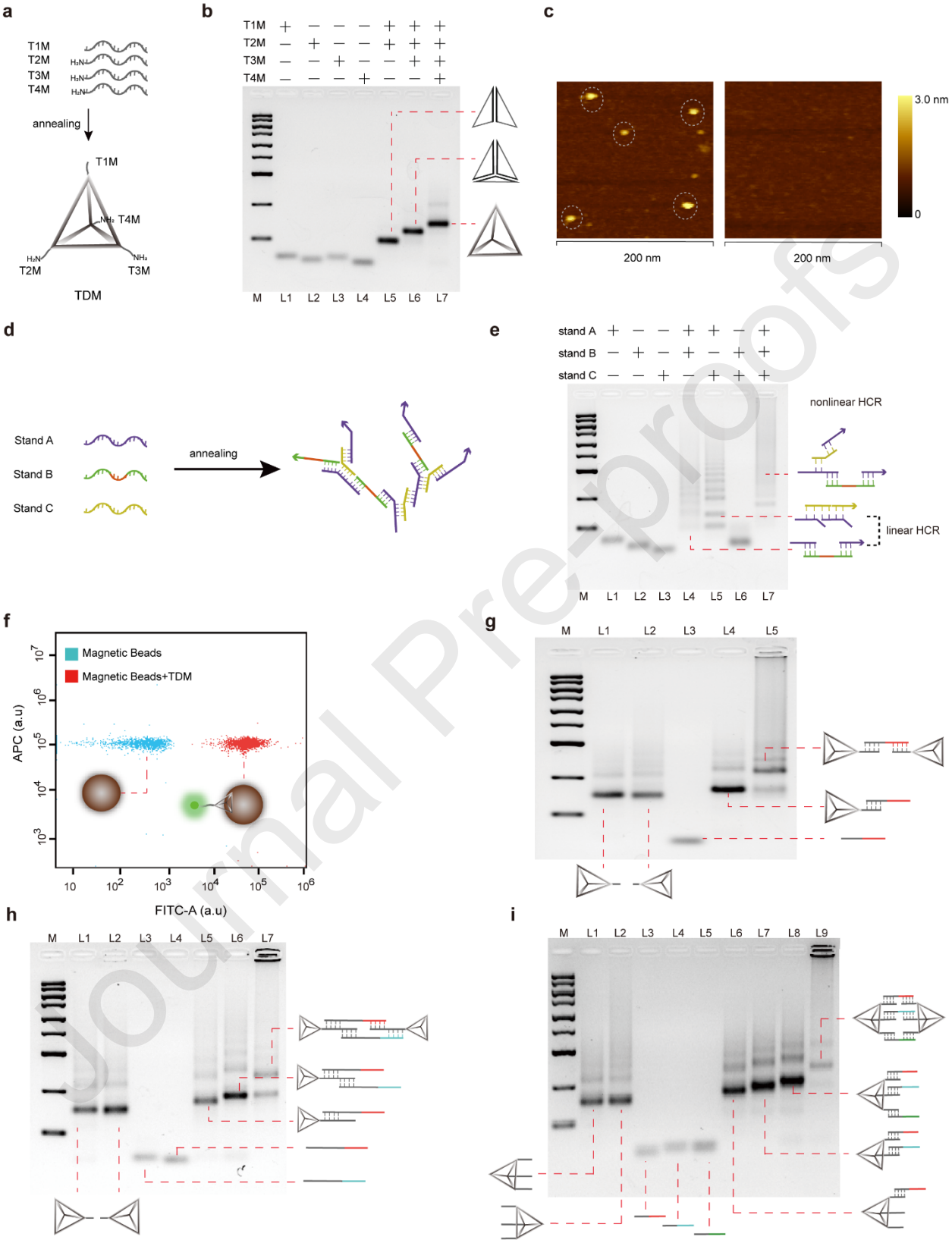
The successful assembly of the DNA tetrahedron and nonlinear HCR are characterized in **Figure 2a-c** and **Figure 2d, e**, respectively. The DNA tetrahedrons (TDM and TDH) consist of four individual strands, respectively (**Figure 2a, Table S1**). Agarose gel electrophoresis analysis revealed that the migration rate of the successfully assembled DNA tetrahedron was slower than that of the DNA dimers and trimers, benefitting from a fast-cooling synthesis method that yields few by-products (**Figure 2b, Figure S1a**). The assembly rate of tetrahedron can be calculated by comparing the intensity of product band with the intensity of all bands in the same lane. Band intensity analysis reveals a tetrahedron assembly rate of over 90%. The images acquired by atomic force microscopy (AFM) display the spatial structure of DNA tetrahedron with a side length of about 5 nm. By contrast, the control ssDNA could not be characterized by AFM due to its unrigid structure. (**Figure 2c**). Nonlinear HCR was synthesized by annealing of three single-stranded DNAs (ssDNAs) (**Figure 2d**), and their positions could be observed by 2% agarose gel electrophoresis (**Figure 2e**). Compared to linear HCR formed by two out of the three ssDNAs, the products of nonlinear HCR exhibited slower migration rate and larger molecular weight (**Figure 2e**). In addition, the formation of TDH-nonlinear HCR complex was also verified by agarose gel electrophoresis (**Figure S1b**). T1M strand was labeled with a green fluorescent dye and the fluorescence intensity of labeled tetrahedron could not be detected by flow cytometry due to its small size. Only when the labeled tetrahedron was attached to the magnetic bead, the enhanced green fluorescence could be detected, which is shown in the figure as the right shift of the FITC signal (**Figure 2f**).

The assemblies of dumbbell lock, double-safety dumbbell lock and triple-safety dumbbell lock have been validated by agarose gel electrophoresis (**Figure 2g, h and i**). Tetrahedrons (TDM and TDH) were pre-assembled and revealed in lane 1 and 2 of each gel image, respectively. An upward movement of the band was observed when adding linker(s) to the TDM. Subsequent addition of TDH to the TDM-linker(s) system produced a band with slower mobility, indicating the formation of dumbbell lock.

In the SMARTLOCK, the nonlinear HCR acts as an initiator to activate the Cas12a: crRNA binary complex. The nonlinear HCR is preassembled and then connected to the three vertices of the tetrahedron to avoid entanglement. Besides, the side length of the tetrahedron is designed to be

5 nm, which ensures the connection of the nonlinear HCR with its three vertices without entanglement. Due to its multi-directionality, the nonlinear HCR binds more efficiently to the Cas12a: crRNA binary complex and thus provides a higher fluorescence signal than the one-dimensional linear HCR (**Figure S2a and b**). In addition, compared with single-stranded nucleic acid, DNA tetrahedrons are ordered and uniformly arranged on the surface of magnetic beads, effectively alleviating the entanglement and monolayer aggregation caused by the self-assembly of single-stranded nucleic acid, thereby improving the binding efficiency and providing higher fluorescent signal (**Figure S2c**). Moreover, the experimental conditions (buffer solution, crRNA concentration, reaction temperature, EDC concentration and incubation time) were optimized to improve the performance of SMARTLOCK (**Figure S3a-e**).

Journal Pre-proofs



Journal Pre-proofs

226

Figure 2. Characterization of SMARTLOCK. (a) Schematic diagram of DNA tetrahedron assembly. (b) Characterization of tetrahedron (TDM) formation by agarose gel electrophoresis. (c) AFM images of DNA tetrahedrons (left) and control ssDNAs (right). (d) Schematic diagram of nonlinear HCR assembly. (e) Nonlinear HCR self-assembly by agarose gel electrophoresis. M: DNA marker, L1: strand A, L2: strand B, L3: strand C, L4: strand A + strand B, L5: strand A + strand C, L6: strand B + strand C, L7: strand A + strand B + strand C. (f) Flow cytometry verification of DNA tetrahedron linked to magnetic beads. (g) Agarose gel electrophoresis analysis of dumbbell lock. M DNA marker, L1: TDM, L2: TDH, L3: linker 1, L4: TDM + linker 1, L5: TDM + linker 1 + TDH. (h) Agarose gel electrophoresis analysis of double-safety dumbbell lock. M: DNA marker, L1: TDM, L2: TDH, L3: linker 1, L4: linker 2, L5: TDM + linker 1, L6: TDM + linker 1 + linker 2, L7: TDM + linker 1 + linker 2 + TDM. (i) Agarose gel electrophoresis analysis of triple-safety dumbbell lock M: DNA marker, L1: TDM, L2: TDH, L3: linker 1, L4: linker 2, L5: linker 3 1, L6: TDM + linker 1, L7: TDM + linker 1 + linker 2, L8: TDM + linker 1 + linker 2 + linker 3 + TDH.

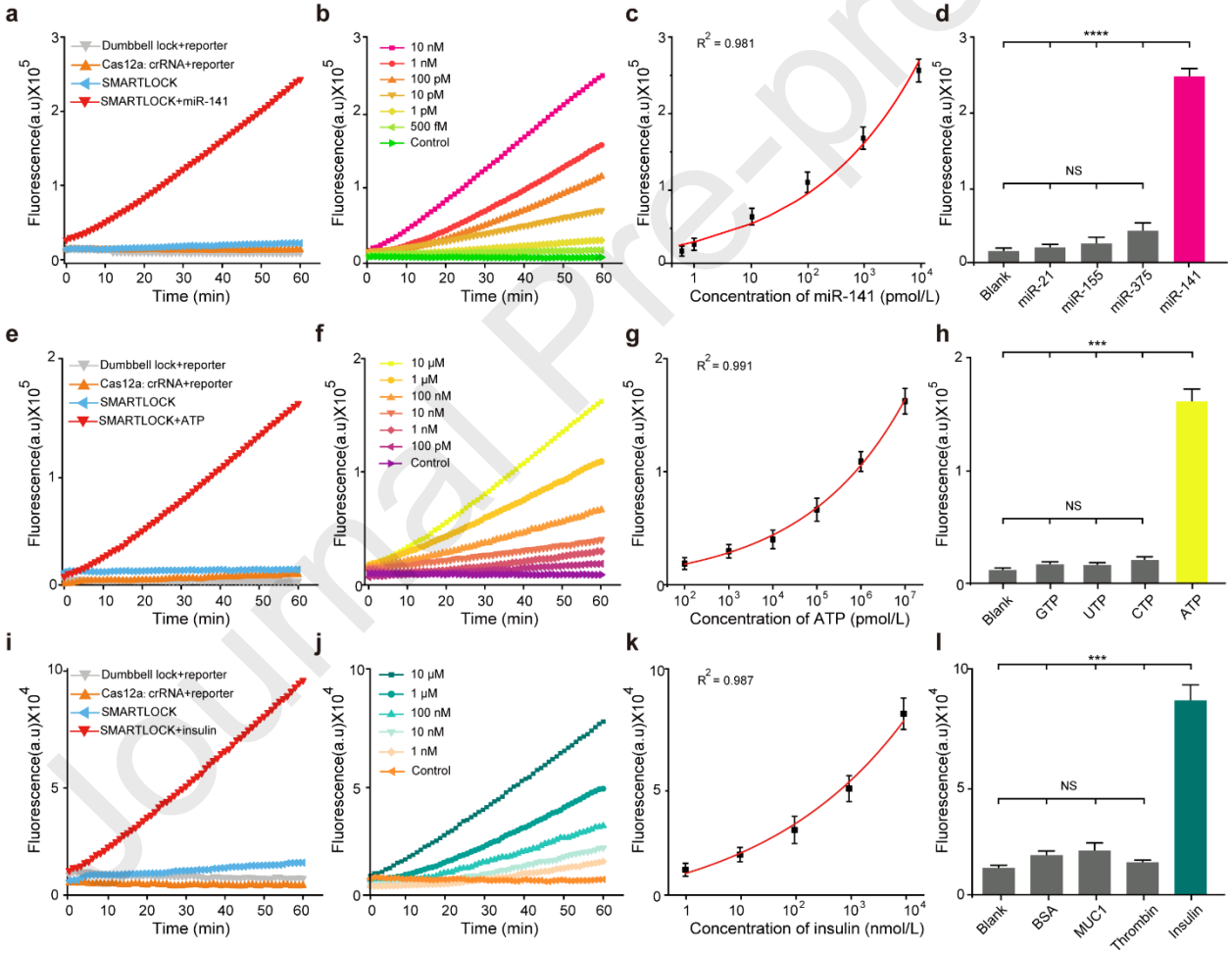
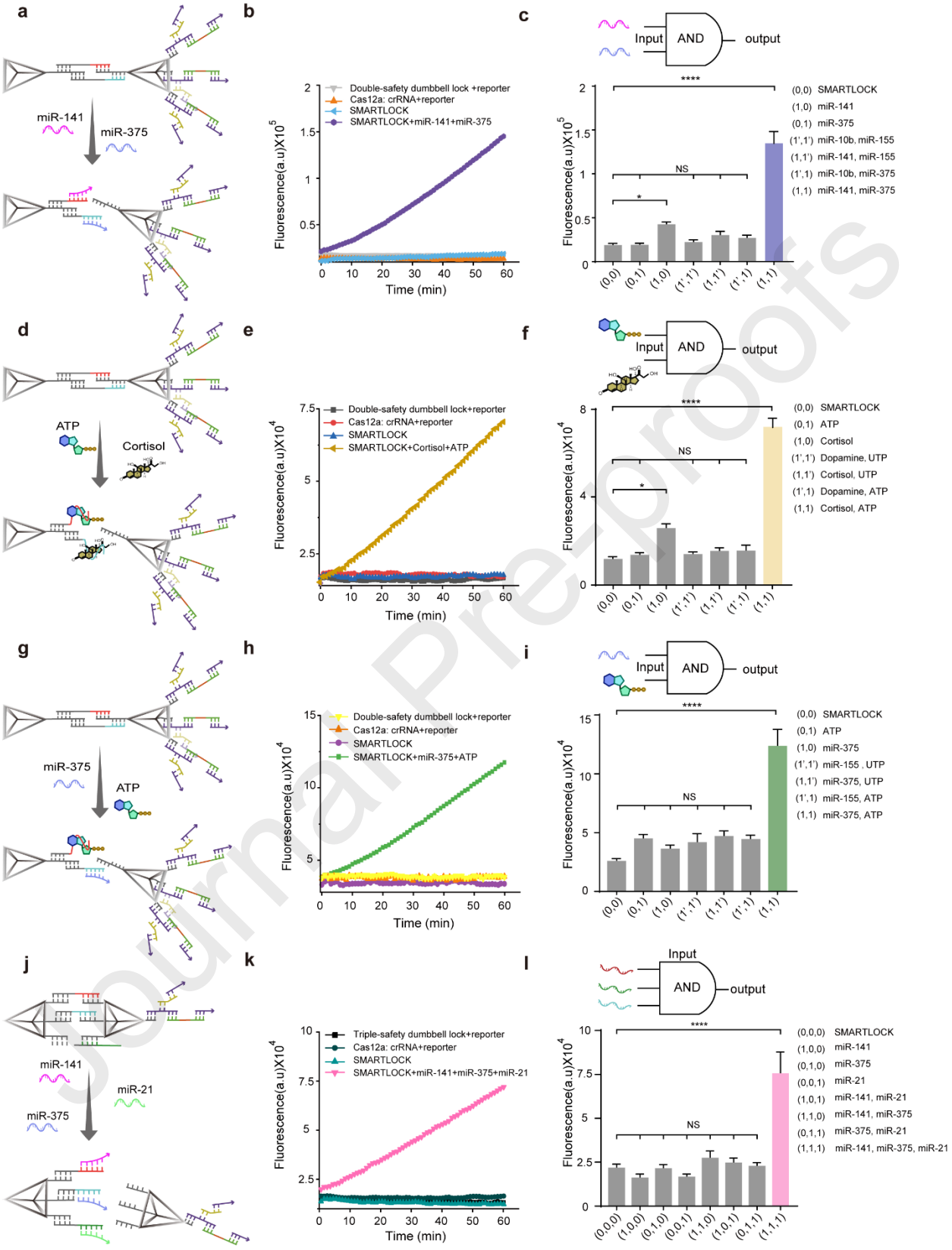


Figure 3. Single-target detection by SMARTLOCK. (a) Feasibility of detection of miR-141 by SMARTLOCK. (b) Real time fluorescence measurement of SMARTLOCK. Different concentrations of miR-141 (500 fM - 10 nM) were introduced into the system at t = 0 min. (c) Linear analysis of miR-141 detection by SMARTLOCK. (d) High specificity was confirmed by

challenging the system with three other miRNAs (miR-21, miR-155 and miR-375). (e) Feasibility of detection of ATP by SMARTLOCK. (f) Real time fluorescence measurement of SMARTLOCK. Different concentrations of ATP (100 pM - 10 μM) were introduced into the system at t = 0 min. (g) Linear analysis of ATP detection by SMARTLOCK. (h) High specificity was confirmed by challenging the system with three other small molecules (GTP, UTP and CTP). (i) Feasibility of detection of insulin by SMARTLOCK. (j) Real time fluorescence measurement of SMARTLOCK. Different concentrations of insulin (1 nM - 10 μM) were introduced into the system at t = 0 min. (k) Linear analysis of insulin detection by SMARTLOCK. (l) High specificity was confirmed by challenging the system with three other proteins (BSA, MUC1 and thrombin). The SMARTLOCK consists of dumbbell lock, Cas12a: crRNA complex and DNA reporter. Data represent mean ± s.d., n = 3, three technical replicates. Paired two-tailed Student's t test, ****$P <$ 0.0001, ns represents non-significance.

3.3. Performance of SMARTLOCK for single target molecules detection

Compared to dumbbell lock, Cas12a: crRNA binary complex and SMARTLOCK alone, a significant fluorescence enhancement was observed in the combination of SMARTLOCK and miR-141, indicating the activation of Cas12a by the released TDH-nonlinear HCR complex (**Figure 3a**). Fluorescence analysis and a calibration curve revealed that the fluorescence intensity of SMARTLOCK increased proportionally to the miR-141 concentration (500 fM-10 nM) with a limit of detection (LOD) as low as 145 fM (**Figure 3b, c**). To challenge the specificity, three other different miRNAs (miR-21, miR-155 and miR-375) were detected at the same concentration (10nM) with miR-141. **Figure 3d** shows that a negligible fluorescence response observed in the presence of miR-21, miR-155 or miR-375 ($P > 0.05$), however, the fluorescence intensity of miR-141 was over 8-fold higher than that of other miRNAs ($P < 0.0001$). In the evaluation of small molecules and proteins, unlike nucleic acid detection, the 5' end of the linker is designed as an aptamer to recognize and bind to target molecule. As shown in **Figure 3e**, the fluorescence signal was significantly increased only in the presence of ATP, while there was nearly no fluorescence response observed in other control groups. The fluorescent intensity exhibited a correlated increase with the elevation of target concentration between 100 pM and 10 μM ($R^2 = 0.991$) (**Figure 3f, g**). The LOD for ATP was as low as 11 pM. To evaluate the specificity of the system, three other ATP analogues molecules (UTP, GTP and CTP) were tested as the interferents. As can be seen in **Figure 3h**, the interferer induced a negligible fluorescence signal ($P > 0.05$). In contrast, the presence of the target ATP resulted in a significant fluorescence enhancement ($P < 0.0001$). Finally, we analyzed the insulin and the feasibility was examined as shown in **Figure 3i**, similarly, a considerable fluorescence increase was induced when the insulin was added to the system. Under optimal conditions, quantitative detection of insulin was realized. The fluorescence intensity was proportional with the concentration of insulin in the range from 1 nM to 10 μM, and a detection limit of 240 pM (**Figure 3j, k**). Similarly, we chose bovine serum albumin (BSA), MUC1 and thrombin as control, a significantly high fluorescent signal was observed only when the target insulin was present ($P < 0.0001$), whereas the presence of other substances exhibited fairly weak fluorescence ($P > 0.05$) (**Figure 3l**). The above results demonstrate the excellent performance of SMARTLOCK for detecting different types (nucleic acids, small molecules and proteins) of target molecules.


a
miR-141
miR-375
b
Double-safety dumbbell lock +reporter
Cas12a: crRNA+reporter
SMARTLOCK
SMARTLOCK+miR-141+miR-375
Fluorescence(a.u)X10^5
Time (min)
c
Input
AND
output
****
NS
*
Fluorescence(a.u)X10^5
(0,0) SMARTLOCK
(1,0) miR-141
(0,1) miR-375
(1',1') miR-10b, miR-155
(1,1') miR-141, miR-155
(1',1) miR-10b, miR-375
(1,1) miR-141, miR-375
d
ATP
Cortisol
e
Double-safety dumbbell lock+reporter
Cas12a: crRNA+reporter
SMARTLOCK
SMARTLOCK+Cortisol+ATP
Fluorescence(a.u)X10^4
Time (min)
f
Input
AND
output
****
NS
*
Fluorescence(a.u)X10^4
(0,0) SMARTLOCK
(0,1) ATP
(1,0) Cortisol
(1',1') Dopamine, UTP
(1,1') Cortisol, UTP
(1',1) Dopamine, ATP
(1,1) Cortisol, ATP
g
miR-375
ATP
h
Double-safety dumbbell lock+reporter
Cas12a: crRNA+reporter
SMARTLOCK
SMARTLOCK+miR-375+ATP
Fluorescence(a.u)X10^4
Time (min)
i
Input
AND
output
****
NS
Fluorescence(a.u)X10^4
(0,0) SMARTLOCK
(0,1) ATP
(1,0) miR-375
(1',1') miR-155 , UTP
(1,1') miR-375, UTP
(1',1) miR-155, ATP
(1,1) miR-375, ATP
j
miR-141
miR-21
miR-375
k
Triple-safety dumbbell lock+reporter
Cas12a: crRNA+reporter
SMARTLOCK
SMARTLOCK+miR-141+miR-375+miR-21
Fluorescence(a.u)X10^4
Time (min)
l
Input
AND
output
****
NS
Fluorescence(a.u)X10^4
(0,0,0) SMARTLOCK
(1,0,0) miR-141
(0,1,0) miR-375
(0,0,1) miR-21
(1,0,1) miR-141, miR-21
(1,1,0) miR-141, miR-375
(0,1,1) miR-375, miR-21
(1,1,1) miR-141, miR-375, miR-21

289

Figure 4. Detection of dual-target and trial-target by SMARTLOCK. (a) Schematic diagram of dual nucleic acids unlocking double-safety dumbbell lock. (b) Feasibility of detection of dual-target by SMARTLOCK. (c) Specificity of SMARTLOCK for detecting dual-target by logic AND gate. (d) Schematic diagram of dual small molecules unlocking double-safety dumbbell lock. (e) Feasibility of detection of dual small molecules by SMARTLOCK. (f) Specificity of SMARTLOCK for detecting dual small molecules by logic AND gate. (g) Schematic diagram of the combination of nucleic acid and small molecule unlocking double-safety dumbbell lock. (h) Feasibility of detection of the combination of nucleic acid and small molecule by SMARTLOCK. (i) Specificity of SMARTLOCK for detecting the combination of nucleic acid and small molecule by logic AND gate. (j) Schematic diagram of triple nucleic acids unlocking triple-safety dumbbell lock. (k) Feasibility of detection of triple nucleic acids by SMARTLOCK. (l) Specificity of SMARTLOCK for detecting triple-target by logic AND gate. The SMARTLOCK consists of double-safety dumbbell lock or triple-safety dumbbell lock, Cas12a: crRNA complex and DNA reporter. Data represent mean ± s.d., n = 3, three technical replicates. Paired two-tailed Student's t test, *$P < 0.05$, ****$P < 0.0001$, ns represents non-significance.

3.4. Performance of SMARTLOCK for dual target molecules detection

To develop a double-safety dumbbell lock, the DNA fragments of the TDM and TDH vertex were designed binding sites to hybridize with two linkers for simultaneous detection of two targets. For an example of detecting two nucleic acids (miR-375 and miR-141), these two linkers simultaneously recognize and hybridize with miR-375 and miR-141, respectively, and the double-safety dumbbell is unlocked resulting in the release of TDH-nonlinear HCR complex. After magnetic separation, the nonlinear HCR products activate the Cas12a to cleave the DNA reporter probe thereby outputting fluorescent signals (**Figure 4a**). The fluorescence signal of SMARTLOCK was significantly increased in the presence of miR-375 and miR-141, compared to other three negative controls (**Figure 4b**). In addition, we applied this approach to logic gates to investigate the specificity using inputs of single target (miR-375 or miR-141), dual non-targets (miR-10b and miR-155), dual targets (miR-375 and miR-141), and combinations of non-target and target (miR-141 and miR-155, miR-10b and miR-375). As we expected, a significantly higher fluorescence signal was observed in (1,1) condition compared to (0,0) control ($P < 0.0001$), while there was no obvious distinction in other inputs except (1,0) condition (**Figure 4c**). We suppose that, in the absence of miR-141 and miR-375, the TDH of the double safety dumbbell lock is tightly held by 29 base pairs, ensuring that the nonlinear HCR products are firmly attached to the magnetic beads through the dumbbell lock. In the case of (1,0), linker 1 unlocks after hybridization with miR-141, leaving only 12 base pairs of connections in the TDH of the double safety dumbbell lock, which may lead to the instability of the whole system and a certain signal leakage (**Figure S4a**). Likewise, SMARTLOCK is also highly modulable, which can detect different kinds of targets by simply switching the recognition domain of linker and T1H. To validate this, two molecular targets (ATP and cortisol) were first chosen (**Figure 4d**). Feasibility analysis showed that the fluorescence intensity of the system elevated with the addition of ATP and cortisol (**Figure 4e**). Logic gates were also applied to SMARTLOCK for the detection of two small molecule targets, and the statistical analysis shows that the fluorescence intensity of (1,1) condition is significantly higher than that of (0,0) control ($P < 0.0001$), while there was no obvious distinction in other inputs except (1,0) condition (**Figure 4f**). The reason is probably that, the TDH of the

double safety dumbbell lock is tightly held by 35 base pairs in the absence of ATP and cortisol. In (1,0) condition, linker 2 unwinds after binding to cortisol, leaving only 14 base pairs of connections in the TDH of the double safety dumbbell lock, possibly resulting in the instability of the whole system and a certain signal leakage (**Figure S4b**). Simultaneous detection of multiple biomarkers could significantly improve the accuracy and reliability of disease diagnosis, however, most of the reported work has only focused on detecting a single type of biomarkers. In this study, we also explored the ability of SMARTLOCK in detecting two different types of biomarkers (ATP and miR-375). Unlocking the double-safety dumbbell lock requires miR-375 to bind to complementary sequences and ATP to bind to its aptamer in the recognition domain of linkers, simultaneously (**Figure 4g**). As shown in **Figure 4h**, SMARTLOCK exhibited an obvious fluorescence only in the presence of both miR-375 and ATP. Logic gate circuit demonstrates the good specificity of SMARTLOCK in detecting two different types of biomarkers ($P < 0.0001$) (**Figure 4i**). The double-safety dumbbell lock has been validated by detecting dual nucleic acid targets, dual small molecule targets and their combinations, opening a new avenue for dual target detection.

3.5. Performance of SMARTLOCK for trial-targets molecules detection

As shown in **Figure 1c** and **Figure 4j**, the triple-safety dumbbell lock consists of three linkers connecting the three vertices of each tetrahedron, the fourth vertex of which is used to conjugate with the magnetic bead and to hybridize with the nonlinear HCR products, respectively. With the simultaneous addition of miR-141, miR-375 and miR-21 to the system, the triple-safety dumbbell lock from inactive to active configuration ensures the downstream reactions to output signals (**Figure 4k**). Similarly, single target input did not elicit a fluorescence increase, but a slight fluorescence increase was caused when two target miRNAs were input simultaneously. Obviously, robust fluorescence intensity can be observed under the condition of co-existence of the three targets ($P < 0.0001$) (**Figure 4l**).

3.6. Performance of SMARTLOCK in complex fluids

One of the biggest challenges with biosensors is their ability to detect biomolecules in complex fluids. To validate the performance of our biosensor in complex biological fluids, the tests were performed in 10% human serum, and three different target molecules (miR-141, ATP and insulin) were chosen. As shown in **Figure S5**, the signal recovery of SMARTLOCK was verified based on spiking 10 nM miR-141, 10 μM ATP, 10 μM insulin in cutsmart buffer and 10% human serum, respectively. Statistical analysis of fluorescence data revealed that the signal from spiked miR-141, ATP and insulin was recovered by 90.2%, 101.5% and 107.9% in 10% human serum, respectively, compared with cutsmart buffer. These results are encouraging for the application of SMARTLOCK to complex biological samples.

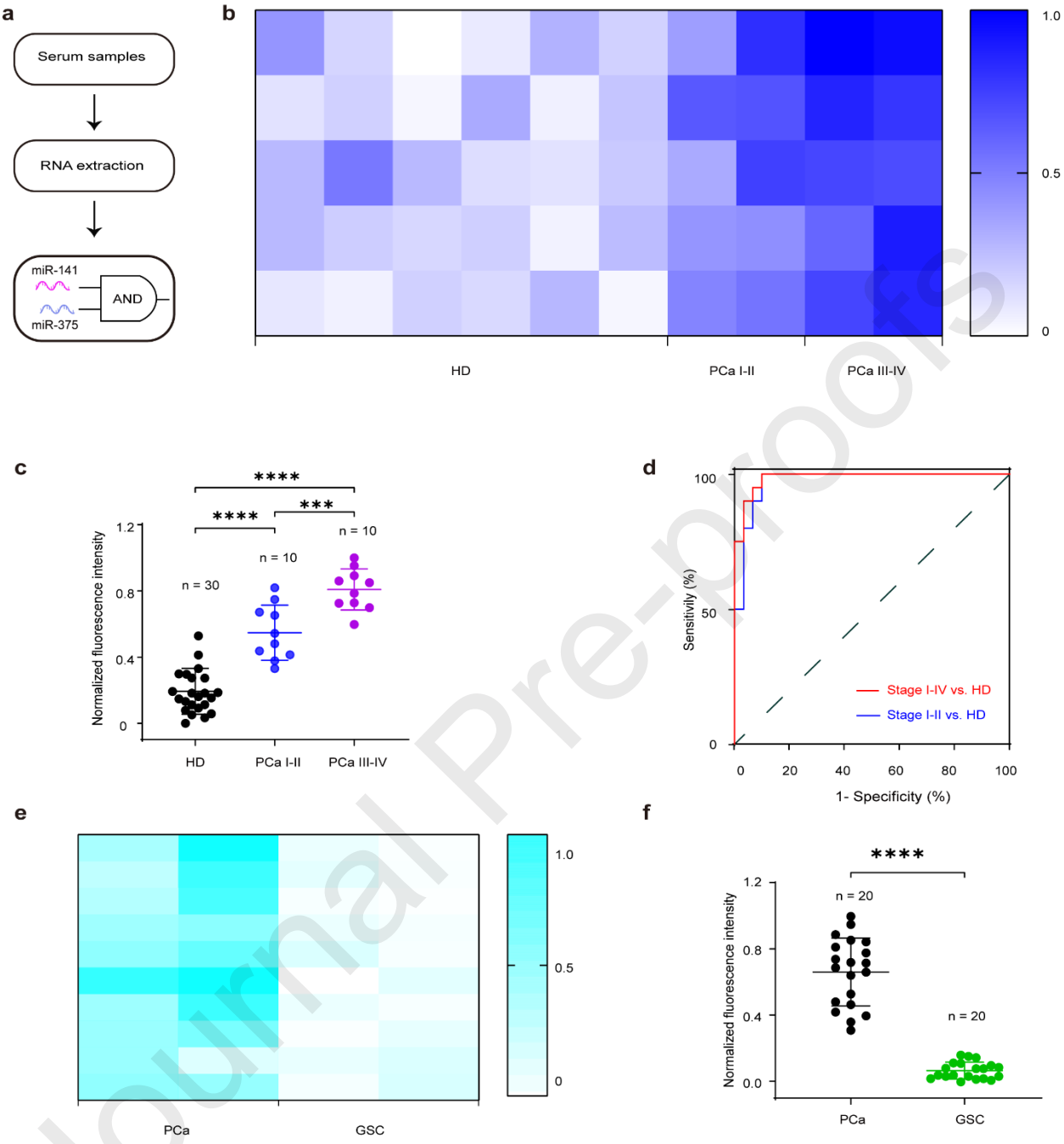


Figure 5. Clinical validation of SMARTLOCK. (a) Schematic diagram of serum sample detection. (b) Heatmap of miR-141 and miR-375 profiles from 30 HDs and 20 PCa patients. (c) Normalized fluorescence intensities of miR-141 and miR-375 expressions in serum of HDs, early stage PCa patients and late stage PCa patients. (d) ROC curve analysis of SMARTLOCK for discriminating PCa patients at stage I-IV, PCa patients at stage I-II from healthy donors, respectively. (e) Heat map of SMARTLOCK for distinguishing PCa patients from GSC patients. (f) Normalized fluorescence intensities of miR-141 and miR-375 expressions in serum of PCa patients and GSC patients. Data represent mean ± s.d., n = 3, three technical replicates. Paired two-tailed Student's t test, ***$P < 0.001$, ****$P < 0.0001$.

Journal Pre-proofs

3.6. PCa patient detection by SMARTLOCK

To investigate the potential clinical utility of the SMARTLOCK in cancer diagnosis (**Figure 5a**), we evaluated the levels of miR-141 and miR-375 in human serum from healthy donors (HDs, n = 30), PCa patients at stage I-II (n = 10) and stage III-IV (n = 10) (**Table S2**). The signal intensity shown in the heatmap increases progressively from HDs to PCa patients at I-II and III-IV (**Figure 5b**). This was no significant overlap of fluorescence signals between healthy donors and early-or late-stage PCa patients, demonstrating that SMARTLOCK allows effective discrimination between healthy donors and PCa patients, even at early stage ($P < 0.001$, **Figure 5c**). Compared PCa patients at I-IV with healthy donors, the receiver operating characteristic (ROC) curve of SMARTLOCK shows an AUC of 0.986 with a sensitivity of 95%, specificity of 93.3% and accuracy of 92.5%. Notably, the ROC curve shows an AUC of 0.973 with a sensitivity of 90%, specificity of 93.3% and accuracy of 90% for PCa patients at I-II compared to healthy donors (**Figure 5d**). In addition, to verify the ability of SMARTLOCK to distinguish different cancers, we also evaluated the abundance of miR-141 and miR-375 in serum samples from Gastric cancer (GSC) patients (n = 20) and PCa patients (n = 20), and the heat map in **Figure 5e** revealed obvious darker color of PCa patients compared to GSC patients. The normalized fluorescence signal showed that the levels of miR-141 and miR-375 in PCa patients were significantly higher than those in GSC patients (**Figure 5f**). Taken together, the SMARTLOCK proves to be a promising tool for early-stage disease diagnosis.

4. Conclusion

In this work, we present a facile and yet powerful biosensor, that integrate DNA tetrahedron, nonlinear HCR with CRISPR-Cas12a system for simultaneous detection of multiple biomarkers of different kinds. The unique nanostructure of DNA tetrahedron realizes the design of double-safety dumbbell lock and triple-safety dumbbell lock for simultaneous detection of dual-target molecules and trial-target molecules, respectively. When challenged with serum sample, SMARTLOCK revealed the necessity of multi-target detection in order to achieve an accurate disease diagnosis, especially for early-stage cancer. The sensitivity, specificity and accuracy of SMARKLOCK based on a panel of two RNAs to detect PCa patients at stage I-II are 90%, 93.3% and 90%, respectively. Although SMARTLOCK is performed with separation step and needs to be redesigned and synthesized according to different targets, it allows for pre-assembly, and does not require complex sample preparation, sophisticated and expensive equipment and especially trained operators, which are required for most of the current molecular diagnostic techniques. Compared with other tetrahedron, nonlinear HCR, and CRISPR-Cas12a strategies, our SMARTLOCK enables multiple molecular detection in complex biofluid (**Table S3**). It is worth noting that the total cost of SMARTLOCK and employed reagents can be as low as $ 0.35 per test. As a multifunctional diagnostic biosensor, SMARTLOCK enlarges the CRISPR-based detection from single nucleic acids to various combinations of nucleic acids, small molecules and proteins. Overall, this new technology represents a promising candidate in the disease diagnostics and therapeutic monitoring.

CRediT authorship contribution statement

Yuqing Zhu: Conceptualization, Methodology, Formal analysis, Investigation, Validation, Writing - original draft. **Xiaohe Zheng:** Investigation, Formal analysis, Writing - original draft. **Rui Zhu:** Validation, Investigation, Formal analysis. **Hongrui Zhao:** Formal analysis. **Hongli Zhai:** Formal analysis. **Feiyang Qian:** Formal analysis, Writing - review & editing. **Tenghua Zhang:** Investigation, Formal analysis, Writing - review & editing. **Zihui Xie:** Formal analysis. **Bowen Jiang:** Formal analysis. **Yan Sheng:** Formal analysis, Writing - review & editing, Supervision. **Jiaming Hu:** Methodology, Conceptualization, Formal analysis, Resources, Writing - review & editing, Supervision, Project administration, Funding acquisition.

Declaration of competing interest

The authors declare that they have no known competing financial interests or personal relationships that could have appeared to influence the work reported in this paper.

Acknowledgment

The authors give special thanks to Prof. Jin Wang from the Institute of Translational Medicine, The First Affiliated Hospital of Shenzhen University for supply of Cas12a protein. This work was supported financially by the Guangdong Provincial Pearl River Talents Program (2019QN01Y725), Science and Technology Program of Guangzhou (202206010108), The Major Program of Ningbo Science and Technology Innovation 2025 (2020Z093), Natural Science Foundation of Guangdong Province (2022A1515010370, 2022A1515011721), and National Natural Science Foundation of China (82000044).

Journal Pre-proofs

References

[1] R. Markewitz, A. Torge, K.P. Wandinger, D. Pauli, J. Dargvainiene, A. Franke, L. Bujanda, J.M. Marimon, J.M. Banales, M.A. Gutierrez-Stampa, B. Nafria, R. Junker, Analysis of SARS-CoV-2 reverse transcription-quantitative polymerase chain reaction cycle threshold values vis-a-vis anti-SARS-CoV-2 antibodies from a high incidence region, Int J Infect Dis 110 (2021) 114-122.

[2] L. Shi, X. Zhao, X. Yan, Y. Liu, Y. Liu, H. Cao, K. Su, C. Wang, S. Gao, Q. Liu, Aggressive disseminated Rhizomucor pusillus infection in a Ph-like acute lymphoblastic leukemia patient: Early detection by cell-free DNA next-generation sequencing, J Infect Chemother 28(3) (2022) 459-464.

[3] H. Zhang, X. Liu, C. Zhang, Y. Xu, J. Su, X. Lu, J. Shi, L. Wang, M.P. Landry, Y. Zhu, M. Lv, X. Mi, A DNA tetrahedral structure-mediated ultrasensitive fluorescent microarray platform for nucleic acid test, Sensors and Actuators B: Chemical 321 (2020).

[4] X. Tan, Q. Chen, H. Zhu, S. Zhu, Y. Gong, X. Wu, Y.C. Chen, X. Li, M.W. Li, W. Liu, X. Fan, Fast and Reproducible ELISA Laser Platform for Ultrasensitive Protein Quantification, ACS Sens 5(1) (2020) 110-117.

[5] Y. Sheng, T. Zhang, S. Zhang, M. Johnston, X. Zheng, Y. Shan, T. Liu, Z. Huang, F. Qian, Z. Xie, Y. Ai, H. Zhong, T. Kuang, C. Dincer, G.A. Urban, J. Hu, A CRISPR/Cas13a-powered catalytic electrochemical biosensor for successive and highly sensitive RNA diagnostics, Biosens Bioelectron 178 (2021) 113027.

[6] Y. Li, Z. Huang, Z. Li, C. Li, R. Liu, Y. Lv, Mass Spectrometric Multiplex Detection of MicroRNA and Protein Biomarkers for Liver Cancer, Anal Chem (2022).

[7] J. Li, K. Xun, L. Zheng, X. Peng, L. Qiu, W. Tan, DNA-Based Dynamic Mimicry of Membrane Proteins for Programming Adaptive Cellular Interactions, J Am Chem Soc 143(12) (2021) 4585-4592.

[8] P. Peng, Y. Du, J. Zheng, H. Wang, T. Li, Reconfigurable Bioinspired Framework Nucleic Acid Nanoplatform Dynamically Manipulated in Living Cells for Subcellular Imaging, Angew Chem Int Ed Engl 58(6) (2019) 1648-1653.

[9] L. Wang, X. Wang, Y. Wu, M. Guo, C. Gu, C. Dai, D. Kong, Y. Wang, C. Zhang, D. Qu, C. Fan, Y. Xie, Z. Zhu, Y. Liu, D. Wei, Rapid and ultrasensitive electromechanical detection of ions, biomolecules and SARS-CoV-2 RNA in unamplified samples, Nat Biomed Eng 6(3) (2022) 276-285.

[10] R. Duangrat, A. Udomprasert, T. Kangsamaksin, Tetrahedral DNA nanostructures as drug delivery and bioimaging platforms in cancer therapy, Cancer Sci 111(9) (2020) 3164-3173.

[11] D. Wang, S. Li, Z. Zhao, X. Zhang, W. Tan, Engineering a Second-Order DNA Logic-Gated Nanorobot to Sense and Release on Live Cell Membranes for Multiplexed Diagnosis and Synergistic Therapy, Angew Chem Int Ed Engl 60(29) (2021) 15816-15820.

Journal Pre-proofs

[12] K. Jiao, B. Zhu, L. Guo, H. Zhou, F. Wang, X. Zhang, J. Shi, Q. Li, L. Wang, J. Li, C. Fan, Programming Switchable Transcription of Topologically Constrained DNA, J Am Chem Soc 142(24) (2020) 10739-10746.

[13] Z. Fan, B. Yao, Y. Ding, D. Xu, J. Zhao, K. Zhang, Rational engineering the DNA tetrahedrons of dual wavelength ratiometric electrochemiluminescence biosensor for high efficient detection of SARS-CoV-2 RdRp gene by using entropy-driven and bipedal DNA walker amplification strategy, Chem Eng J 427 (2022) 131686.

[14] Y.-H. Liu, J.-X. Liu, J.-L. Gao, H.-W. Tang, C.-Y. Li, A dual DNA tetrahedrons and MnO2 nanosheets sustained entropy-driven DNA amplifier enables high-performance operation in live cells and bodies under a light-gated manner, Chemical Engineering Journal 438 (2022).

[15] X. Qu, M. Xiao, F. Li, W. Lai, L. Li, Y. Zhou, C. Lin, Q. Li, Z. Ge, Y. Wen, H. Pei, G. Liu, Framework Nucleic Acid-Mediated Pull-Down MicroRNA Detection with Hybridization Chain Reaction Amplification, ACS Appl Bio Mater 1(3) (2018) 859-864.

[16] P. Ji, G. Han, Y. Huang, H. Jiang, Q. Zhou, X. Liu, D. Kong, Ultrasensitive ratiometric detection of Pb(2+) using DNA tetrahedron-mediated hyperbranched hybridization chain reaction, Anal Chim Acta 1147 (2021) 170-177.

[17] Z. Zeng, R. Zhou, R. Sun, X. Zhang, Z. Cheng, C. Chen, Q. Zhu, Nonlinear hybridization chain reaction-based functional DNA nanostructure assembly for biosensing, bioimaging applications, Biosens Bioelectron 173 (2020) 112814.

[18] X. Hun, Y. Meng, S. Wang, Z. Mei, X. Luo, Concatenated logic gates by amplified chemiluminescence of hemin/G-Quadruplex DNAzyme based on a nonlinear hybridization chain reaction, Sensors and Actuators B: Chemical 246 (2017) 734-739.

[19] D. Wilbie, J. Walther, E. Mastrobattista, Delivery Aspects of CRISPR/Cas for in Vivo Genome Editing, Acc Chem Res 52(6) (2019) 1555-1564.

[20] S. Jain, G. Xun, S. Abesteh, S. Ho, M. Lingamaneni, T.A. Martin, I. Tasan, C. Yang, H. Zhao, Precise Regulation of Cas9-Mediated Genome Engineering by Anti-CRISPR-Based Inducible CRISPR Controllers, ACS Synth Biol 10(6) (2021) 1320-1327.

[21] M.M. Kaminski, O.O. Abudayyeh, J.S. Gootenberg, F. Zhang, J.J. Collins, CRISPR-based diagnostics, Nat Biomed Eng 5(7) (2021) 643-656.

[22] S.Y. Li, Q.X. Cheng, J.K. Liu, X.Q. Nie, G.P. Zhao, J. Wang, CRISPR-Cas12a has both cis- and trans-cleavage activities on single-stranded DNA, Cell Res 28(4) (2018) 491-493.

[23] T. Li, R. Hu, J. Xia, Z. Xu, D. Chen, J. Xi, B.F. Liu, J. Zhu, Y. Li, Y. Yang, M. Liu, G-triplex: A new type of CRISPR-Cas12a reporter enabling highly sensitive nucleic acid detection, Biosens Bioelectron 187 (2021) 113292.

[24] M. Qing, S.L. Chen, Z. Sun, Y. Fan, H.Q. Luo, N.B. Li, Universal and Programmable Rolling Circle Amplification-CRISPR/Cas12a-Mediated Immobilization-Free Electrochemical Biosensor,

Anal Chem 93(20) (2021) 7499-7507.

[25] R. Nouri, Y. Jiang, X.L. Lian, W. Guan, Sequence-Specific Recognition of HIV-1 DNA with Solid-State CRISPR-Cas12a-Assisted Nanopores (SCAN), ACS Sens 5(5) (2020) 1273-1280.

[26] M. Liang, Z. Li, W. Wang, J. Liu, L. Liu, G. Zhu, L. Karthik, M. Wang, K.F. Wang, Z. Wang, J. Yu, Y. Shuai, J. Yu, L. Zhang, Z. Yang, C. Li, Q. Zhang, T. Shi, L. Zhou, F. Xie, H. Dai, X. Liu, J. Zhang, G. Liu, Y. Zhuo, B. Zhang, C. Liu, S. Li, X. Xia, Y. Tong, Y. Liu, G. Alterovitz, G.Y. Tan, L.X. Zhang, A CRISPR-Cas12a-derived biosensing platform for the highly sensitive detection of diverse small molecules, Nat Commun 10(1) (2019) 3672.

[27] Y. Xiong, J. Zhang, Z. Yang, Q. Mou, Y. Ma, Y. Xiong, Y. Lu, Functional DNA Regulated CRISPR-Cas12a Sensors for Point-of-Care Diagnostics of Non-Nucleic-Acid Targets, J Am Chem Soc 142(1) (2020) 207-213.

[28] C. Niu, C. Wang, F. Li, X. Zheng, X. Xing, C. Zhang, Aptamer assisted CRISPR-Cas12a strategy for small molecule diagnostics, Biosens Bioelectron 183 (2021) 113196.

[29] Y. Lv, Y. Sun, I. Mahmood Khan, Q. Li, Y. Zhou, L. Yue, Y. Zhang, Z. Wang, Locking-DNA network regulated CRISPR-Cas12a fluorescent aptasensor based on hollow flower-like magnetic MoS2 microspheres for sensitive detection of sulfadimethoxine, Chemical Engineering Journal 459 (2023).

[30] C. Wang, C. Han, X. Du, W. Guo, Versatile CRISPR-Cas12a-Based Biosensing Platform Modulated with Programmable Entropy-Driven Dynamic DNA Networks, Anal Chem 93(38) (2021) 12881-12888.

[31] P. Porzycki, E. Ciszkowicz, M. Semik, M. Tyrka, Combination of three miRNA (miR-141, miR-21, and miR-375) as potential diagnostic tool for prostate cancer recognition, Int Urol Nephrol 50(9) (2018) 1619-1626.

[32] J.C. Brase, M. Johannes, T. Schlomm, M. Falth, A. Haese, T. Steuber, T. Beissbarth, R. Kuner, H. Sultmann, Circulating miRNAs are correlated with tumor progression in prostate cancer, Int J Cancer 128(3) (2011) 608-16.

[33] S. Cai, T. Pataillot-Meakin, A. Shibakawa, R. Ren, C.L. Bevan, S. Ladame, A.P. Ivanov, J.B. Edel. Single-molecule amplification-free multiplexed detection of circulating microRNA cancer biomarkers from serum, Nat Commun 12(1) (2021) 3515.

Single-molecule amplification-free multiplexed detection of circulating microRNA cancer biomarkers from serum, Nat Commun 12(1) (2021) 3515.

[34] N. Xue, S. Wu, Z. Li, X. Miao, Ultrasensitive and label-free detection of ATP by using gold nanorods coupled with enzyme assisted target recycling amplification, Anal Chim Acta 1104 (2020) 117-124.

[35] J.E. An, K.H. Kim, S.J. Park, S.E. Seo, J. Kim, S. Ha, J. Bae, O.S. Kwon, Wearable Cortisol Aptasensor for Simple and Rapid Real-Time Monitoring, ACS Sens 7(1) (2022) 99-108.

Journal Pre-proofs

[36] C. Sabu, T.K. Henna, V.R. Raphey, K.P. Nivitha, K. Pramod, Advanced biosensors for glucose and insulin, Biosens Bioelectron 141 (2019) 111201.

Declaration of competing interest

The authors declare that they have no known competing financial interests or personal relationships that could have appeared to influence the work reported in this paper.

Highlights

- A CRISPR-powered multifunctional detection biosensor was developed.
- Three DNA nanodumbbell lock structures were used for multiple molecular detection.
- Early -stage prostate cancer patients could be distinguished from healthy people.
- The DNA nanodumbbell locks were able to assembled in advance, allowing its application even in resource limited settings.

Journal Pre-proofs